

NCAR Global Model Topography Generation Software for Unstructured Grids

Julio T. Bacmeister¹, Peter H. Lauritzen¹, and Patrick F. Callaghan¹

¹National Center for Atmospheric Research, 1850 Table Mesa Drive, Boulder, Colorado, USA

Correspondence to: Peter Hjort Lauritzen
(pel@ucar.edu)

Abstract. TEXT

1 Introduction

CURRENTLY TEXT HAS BEEN COPY-PASTED FROM
DOE PROPOSAL - NEEDS RE-ORDERING ETC.

- topographic input data in models:
 - resolved-scale elevation Φ_s which usually needs to be smoothed
 - SGH: gravity wave drag
 - anisotropic gravity wave drag (dominant sub-grid-scale orientation)
 - SGH30: turbulent mountain stress
 - LANDFRAC
- Should we mention dynamic topography in the CESM (Jeremy Fyke, LANL).

Accurate representation of the impact of orography on atmospheric flow is crucial for Earth system modeling (ESM). For example, on the regional scale the hydrological cycle is closely linked to topography and, on the planetary scale, waves associated with the mid-latitude jets are very susceptible to the effective drag caused by mountains (e.g., Lott and Miller, 1997). Atmospheric blocking producing heat waves and droughts as well as atmospheric rivers are closely related to topographic forcing. Despite the fact that surface elevation is known globally to within a meter (or less), its representation in numerical models remains a challenge.

In this paper we present a versatile software package for generating topographic model input data....

2 Method

2.1 ‘Raw’ elevation data

The ‘raw’ elevation data is usually from a digital elevation model (DEM) such as the GTOPO30; a 30 arc second global dataset from the United States Geological Survey (USGS; Gesch and Larson, 1998) defined on an approximately 1km regular latitude-longitude grid. Several newer, more accurate, and locally higher resolution elevation datasets are available such as GLOBE (GLOBE Task Team and others, 1999) and the NASA Shuttle Radar Topographic Mission (SRTM) DEM data (Farr et al., 2007). The SRTM data, however, is only near-global (up to 60° North and South).

2.2 Continuous: separation of scales

The separation of scales is, in continuous space, conveniently introduced using spherical harmonics. Assume that elevation (above sea level) is a smooth continuous function in which case it can be represented by a convergent expansion of spherical harmonic functions of the form

$$h(\lambda, \theta) = \sum_{m=-\infty}^{\infty} \sum_{n=|m|}^{\infty} \psi_{m,n} Y_{m,n}(\lambda, \theta), \quad (1)$$

(e.g., Durran, 2010) where λ and θ are longitude and latitude, respectively, $\psi_{m,n}$ are the spherical harmonic coefficients. Each spherical harmonic function is given in terms of the associated Legendre polynomial $P_{m,n}(\theta)$:

$$Y_{m,n} = P_{m,n}(\theta) e^{im\lambda} \quad (2)$$

where m is the zonal wavenumber and $m - |n|$ is the number of zeros between the poles and can therefore be interpreted as meridional wavenumber.

55 For the separation of scales of the variance of sub-grid-scale elevation the spherical harmonic expansion is truncated at wavenumber M

$$h^{(M)}(\lambda, \theta) = \sum_{m=-M}^{\infty} \sum_{n=|m|}^M \psi_{m,n}^{(M)} Y_{m,n}(\lambda, \theta), \quad (3)$$

60 where a triangular truncation, which provides a uniform spatial resolution over the entire sphere, is used.

65 Let $h^{(tgt)}(\lambda, \theta)$ be a continuous representation of the elevation containing the spatial scales of the target grid. We do not write that in terms of spherical harmonics as the target grid may be variable resolution and therefore contains different spatial scales in different parts of the domain.

For each target grid cell Ω_k , $k = 1, \dots, N_t$, where N_t is the number of target grid cells, define the variances

$$\begin{aligned} \text{Var}_{\Omega_k}^{(tms)} &= \iint_{\Omega_k} \left[h^{(M)}(\lambda, \theta) - h(\lambda, \theta) \right]^2 \cos(\theta) d\lambda d\theta, \quad (4) \\ \text{Var}_{\Omega_k}^{(gwd)} &= \iint_{\Omega_k} \left[h^{(tgt)}(\lambda, \theta) - h^{(M)}(\lambda, \theta) \right]^2 \cos(\theta) d\lambda d\theta \end{aligned}$$

70 So $\text{Var}_{\Omega_k}^{(tms)}$ is the variance of elevation on scales below wavenumber M and $\text{Var}_{\Omega_k}^{(gwd)}$ is the variance of elevation on scales larger than wavenumber M and below the target grid scale.

75 [julio: continuous definition of dominant orientation of orography with this notation?]

2.3 Discrete

The separation of scales is done through the use of a quasi-isotropic gnomonic cubed-grid grid in a two-step regridding procedure, that is, binning from source grid Λ to intermediate grid A (separation of scales) to target grid Ω .

80 Any quasi-uniform spherical grid could, in theory, be used for the separation of scales. For reasons that will become clear we have chosen to use a gnomonic cubed-sphere grid resulting from an equi-angular gnomonic (central) projection

$$x = r \tan \alpha \quad \text{and} \quad y = r \tan \beta; \quad \alpha, \beta \in \left[-\frac{\pi}{4}, \frac{\pi}{4} \right], \quad (6)$$

(Ronchi et al., 1996) where α and β are central angles in each coordinate direction, $r = R/\sqrt{3}$ and R is the radius of the Earth. A point on the sphere is identified with the three-element vector (x, y, ν) , where ν is the panel index. Hence the physical domain S (sphere) is represented by the gnomonic (central) projection of the cubed-sphere faces, $\Omega^{(\nu)} = [-1, 1]^2$, $\nu = 1, 2, \dots, 6$, and the non-overlapping panel domains $\Omega^{(\nu)}$ span the entire sphere: $S = \bigcup_{\nu=1}^6 \Omega^{(\nu)}$. The cube edges, however, are discontinuous. Note that any straight line on the gnomonic projection (x, y, ν) corresponds to a great-circle arc on the sphere. In

100 the discretized scheme we let the number of cells along a coordinate axis be N_c so that the total number of cells in the global domain is $6 \times N_c^2$. The grid lines are separated by the same angle $\Delta\alpha = \Delta\beta = \frac{\pi}{2N_c}$ in each coordinate direction.

For notational simplicity the cubed-sphere cells are identified with one index i and the relationship between i and $(icube, jcube, \nu)$ is given by

$$i = icube + (jcube - 1) N_c + (\nu - 1) N_c^2, \quad (7)$$

where $(icube, jcube) \in [1, \dots, N_c]^2$ and $\nu \in [1, 2, \dots, 6]$. In terms of central angles the cubed-sphere grid cell i is defined as

$$A_i = [(icube - 1)\Delta\alpha - \pi/4, icube\Delta\alpha - \pi/4] \times [(jcube - 1)\Delta\beta - \pi/4, jcube\Delta\beta - \pi/4], \quad (8)$$

110 and ΔA_i denotes the spherical area. A formula for the spherical area ΔA_i of a grid cell on the gnomonical cubed-sphere grid can be found in Appendix C of Lauritzen and Nair (2008) (note that equation C3 is missing \cos on the right-hand side). A quasi-uniform approximately 3km resolution is obtained by using $N_c = 3000$. For more details on the construction of the gnomonic grid see, e.g., Lauritzen et al. (2010).

2.3.1 Step 1: raw elevation data to intermediate cubed-sphere grid ($\Lambda \rightarrow A$)

The ‘raw’ elevation data is usually from a digital elevation model (DEM) such as the GTOPO30 30 arc second global dataset from the United States Geological Survey (USGS Gesch and Larson, 1998) defined on an approximately 1km regular latitude-longitude grid. Several newer and higher resolution elevation datasets are available such as the NASA Shuttle Radar Topographic Mission (SRTM) DEM data (Farr et al., 2007). The SRTM data, however, is only near-global (up to 60° North and South). In the remainder of this paper we assume that the raw elevation data is the USGS 30 arc second data.

130 The center of the regular latitude-longitude grid cells are denoted $(\lambda_{ilon}, \theta_{jlat})$, $ilon = 1, \dots, nlon$, $jlat = 1, \dots, nlat$. For the USGS dataset used here $nlon = 43200$ and $nlat = 21600$. As for the cubed-sphere we use one index j to reference the grid cells

$$j = ilon + (jlat - 1) \times nlon, \quad j \in [1, \dots, N_r], \quad (9)$$

135 where $N_r = nlon \times nlat$. The spherical area of grid cell Λ_j is denoted $\Delta\Lambda_j$ and the average elevation in cell j is given by $\bar{h}_j^{(usgs)}$

This data is binned to the cubed-sphere intermediate grid by identifying in which gnomonic cubed-sphere grid cell $(\lambda_{ilon}, \theta_{jlat})$ is located. Due to the ‘Cartesian’-like structure of the cubed-sphere grid the search algorithm is straightforward:

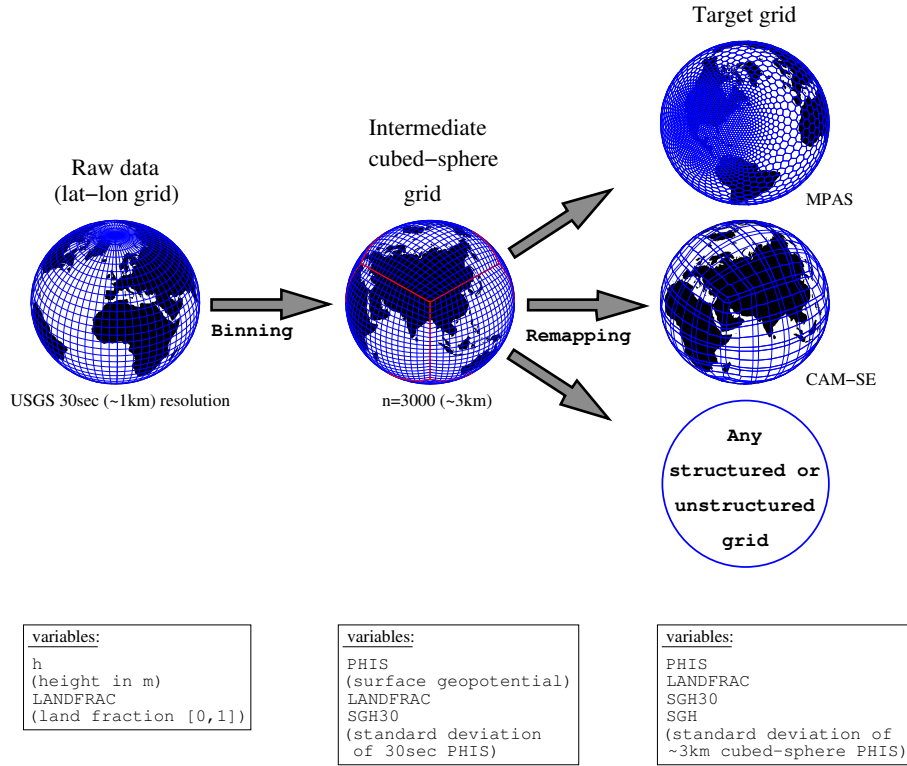


Figure 1. A schematic showing the regridding procedure.

- use the transformation from latitude-longitude coordinates to central angle coordinates described in the Appendix of Nair et al. (2005) to compute the central angles (α, β) corresponding to the mid-point of the latitude-longitude grid cell $(\lambda_{ilon}, \theta_{lat})$. [more details on algorithm z]
- the indices of the cubed-sphere cell in which the center of the latitude-longitude grid cell is located is given by

$$\begin{aligned} icube &= \text{CEILING}\left(\frac{\alpha + \frac{\pi}{4}}{\Delta\alpha}\right), \\ jcube &= \text{CEILING}\left(\frac{\beta + \frac{\pi}{4}}{\Delta\beta}\right), \end{aligned}$$

where the $\text{CEILING}(x)$ function returns the smallest integer not less than x .

The set of indices for which center points of regular latitude-longitude grid cells are located in gnomonic cubed-sphere cell A_i is denoted \mathbb{S}_i . Note that since the USGS dataset is higher resolution than the cubed-sphere \mathbb{S}_i is guaranteed to be non-empty. Through this binning process the approximate average elevation in cubed-sphere cell i becomes

$$\bar{h}_i^{(cube)} = \frac{1}{\Delta A_i} \sum_{j \in \mathbb{S}_i} \bar{h}_j^{(usgs)} \Delta \Lambda_j. \quad (10)$$

The binning process is straight forward since the cubed-sphere grid is essentially an equidistant Cartesian grid on each panel in terms of the central angle coordinates. This step could be replaced by rigorous remapping in terms of overlap areas between the regular latitude-longitude grid and the cubed-sphere grid using the geometrically exact algorithm of (Ullrich et al., 2009) optimized for the regular latitude-longitude and gnomonic cubed-sphere grid pair or the more general remapping algorithm called SCRIP (Jones, 1999).

The sub-grid-scale variance of elevation with respect to the cubed-sphere grid cell i is

$$Var_i^{(tms)} = \frac{1}{\Delta A_i} \sum_{j \in \mathbb{S}_i} \left(\bar{h}_i^{(cube)} - \bar{h}_j^{(usgs)} \right)^2 \Delta \Lambda_j. \quad (11)$$

- mention the changes to raw data: Caspian sea, Antarctica (why are these changes made?)

TODO: show a Figure illustrating the amount of smoothing performed by the binning!

2.3.2 Step 2: cubed-sphere grid to target grid ($A \rightarrow \Omega$)

The cell averaged values of elevation and sub-grid-scale variances ($Var^{(tms)}$ and $Var^{(gwd)}$) on the target grid are computed by rigorously remapping the variables from the cubed-sphere grid to the target grid. The remapping is performed

using CSLAM (Conservative Semi-LAgrangian Multi-tracer transport scheme) technology (Lauritzen et al., 2010) that has the option for performing higher-order remapping. It is possible to use large parts of the CSLAM technology since the source grid is a gnomonic cubed-sphere grid hence instead of remapping between the gnomonic cubed-sphere grid and a deformed Lagrangian grid, as done in CSLAM transport, the remapping is from the gnomonic cubed-sphere grid to any target grid constructed from great-circle arcs (the target grid ‘plays the role’ of the Lagrangian grid). However, a couple of modifications were made to the CSLAM search algorithm. First of all, the target grid cells can have an arbitrary number of vertices whereas the CSLAM transport search algorithm assumes that the target grid consists of quadrilaterals and the number of overlap areas are determined by the deformation of the transporting velocity field. In the case of the remapping needed in this application the target grid consists of polygons with any number of vertices and the search is not constrained by the physical relation between regular and deformed upstream quadrilaterals. Secondly, the CSLAM search algorithm for transport assumes that the target grid cells are convex which is not necessarily the case for topography target grids. The CSLAM search algorithm has been modified to support non-convex cells that are, for example, encountered in variables resolution CAM-SE; essentially that means that any target grid cell may cross a gnomonic isoline (source grid line) more than twice as is the case for transport.

Let the target grid consist of N_t grid cells Ω_k , $k = 1, \dots, N_t$ with associated spherical area $\Delta\Omega_k$. The search algorithm for CSLAM is used to identify overlap areas between the target grid cell Ω_k and the cubed-sphere grid cells A_ℓ , $\ell = 1, \dots, N_c$. Denote the overlap area between Ω_k and A_ℓ

$$\Omega_{k\ell} = \Omega_k \cap A_\ell, \quad (12)$$

and let \mathbb{L}_k denote the set of indices for which $\Omega_k \cap A_\ell$, $\ell = 1, \dots, N_c$, is non-empty. Then the average elevation and variance used for TMS in target grid cell k are given by

$$\bar{h}_k^{(targ)} = \frac{1}{\Delta\Omega_k} \sum_{\ell \in \mathbb{L}_k} \bar{h}_\ell^{(cube)} \Delta\Omega_{k\ell}, \quad (13)$$

$$\bar{Var}_k^{(tms)} = \frac{1}{\Delta\Omega_k} \sum_{\ell \in \mathbb{L}_k} \bar{Var}_\ell^{(tms)} \Delta\Omega_{k\ell}, \quad (14)$$

respectively. The variance of the cubed-sphere data $\bar{h}^{(cube)}$ with respect to the target grid cell average values $\bar{h}^{(targ)}$ is given by

$$\bar{Var}_k^{(sgb)} = \frac{1}{\Delta\Omega_k} \sum_{\ell \in \mathbb{L}_k} (\bar{h}_k^{(targ)} - \bar{h}_\ell^{(cube)})^2 \Delta\Omega_{k\ell}, \quad (15)$$

2.4 Smoothing of Φ_s

When performing a spectral analysis of the raw elevation data, it is clear that Earth’s topography decreases quite slowly

with increasing wave number Balmino (see, e.g., 1993). Consequently, there will always be a non-negligible spectral component of orography present near the grid scale at current and any foreseeable model resolution. It is common practice not to force the highest wave numbers directly in the model to alleviate obvious spurious noise (e.g. Navarra et al., 1994; Lander and Hoskins, 1997). Hence the raw topographic data is filtered to remove the highest wave numbers. There seem to be no standardized procedure, for example a test case suite, to objectively select level of smoothing and filtering method.

Modeling groups, with the exception of the UK Met Office (Webster et al., 2003), rarely publish their smoothing procedures and criteria for choosing one level of smoothing over another. It is likely that qualitative methods are used such as the elimination of visible noise in, e.g. vertical velocity, near orography rather than quantitative diagnostics. The amount of smoothing necessary to remove spurious noise in, e.g. vertical velocity, depends on the amount of inherent or explicit numerical diffusion in the dynamical core (e.g., Lauritzen et al., 2011). In the NCAR-DOE CESM (Community Earth System Model) CAM-FV (Community Atmosphere Model - Finite-Volume; Lin, 2004) the highest wave-numbers are removed by mapping Φ_s (surface geopotential) to a regular latitude-longitude grid that is half the resolution of the desired model resolution, and then mapped back to the model grid by one-dimensional remaps along latitudes and longitudes, respectively, using the PPM (Piecewise Parabolic Method) with monotone filtering. In CAM-SE (Community Atmosphere Model - Spectral-Elements; Dennis et al., 2012; Neale et al., 2010) the surface geopotential is smoothed by multiple applications of the CAM-SE Laplace operator combined with a bounds preserving limiter. Figure 4 shows different levels of smoothing of surface height for CAM-SE and for comparison CAM-FV. It can clearly be seen that there are large differences between the height of the mountains used in the dynamical core.

While it is necessary to smooth topography to remove spurious grid-scale noise, it introduces two problems. Filtering will typically raise ocean points near step orography to non-zero elevation. Perhaps the most striking example is the Andes mountain range that extends one or two grid cells into the Pacific after the filtering operation (see, e.g., Figure ?? right). Ocean and land points are treated separately in weather/climate models so raised sea-points may potentially be problematic. Secondly, the filtering will generally reduce the height of local orographic maxima and given the importance of barrier heights in atmospheric dynamics, this could be a problem for the global angular momentum budget and could fundamentally change the flow.

To capture the barrier effect (blocking) that is sub-grid scale with respect to the smoothed orography, one may use *envelope orography* that adjusts the surface height with sub-grid scale orographic variance (Wallace et al., 1983). Loosely speaking, the peak heights are raised. A similar approach, but implemented as variational filtering, is taken in Rutt et al.

(2006); this method also imposes additional constraints such as enforcing zero elevation over ocean masks.

As mentioned above it is not straight forward to determine how to smooth orography. One approach is to try different filtering methods in the full model and evaluate the results in weather forecasts or longer climate simulations (Navarra et al., 1994; Bouteloup, 1995, 1996). While this approach is certainly valuable, clearly the size of the Gibbs oscillations in global spectral models is reduced by smoothing orography, it does not take into account the interaction between the resolved-scale flow (dynamical core) and parameterizations of sub-grid scale processes (e.g., gravity wave drag, turbulent mountain stress). This interaction can be difficult to predict and commonly the sub-grid scale parameterization have been tuned over a number of years with the ‘default’ smoothed surface elevation. Hence, this methodology runs the risk of deeming one smoothing less accurate than another due to lack of optimum tuning (and/or complexity) of the parameterizations.

Another approach is to use idealized simulation with no parameterizations to determine what scales are adequately resolved and which are poorly resolved. Davies and Brown (2001) kept the physical scale of an idealized two-dimensional and three-dimensional isolated hill fixed and observed how the coarser resolution results differ from the high-resolution simulation. This can then provide guide-lines on how to smooth orography in the full model. Similar idealized (shallow water) experiments were used in Rutt et al. (2006) to optimally smooth orography. While these idealized tests provide a ‘cleaner’ approach to smoothing terrain, they do not consider the coupling with sub-grid scale processes.

Describe internal smoothing algorithm ,,,

2.4.1 Algorithm for determining the dominant orientation of sub-grid orography

Our algorithm for determining the dominant orientation of sub-grid orography is relatively straightforward. We begin with 3 km topography on the intermediate cubed-sphere grid and compute an extension of each panel on the cubed-sphere via high-order interpolation so that each panel can numerically be treated essentially as a Cartesian computational domain. An outer/model scale (L) is selected. A high-pass filter is optionally applied to remove larger scales. We then take a square of orography $h(x, y)$ with dimension L and rotate it through 16 test angles ξ_i . ‘Padding’ is used to avoid corner effects. In each test rotation a ‘Y’ average is taken to generate a ridge profile $h_i(x)$ at angle ξ_i . The ratio of the variance of h_i to the total 2D variance in $h(x, y)$ is computed. The angle for which this ratio is greatest is designated as the dominant topographic orientation for the sub-grid topography in the $L \times L$ domain of $h(x, y)$. This is done at regular intervals separated by L over the entire globe. The angle and other topographic parameters can then be mapped from the cubed sphere grid with resolution L to arbitrary model grids using

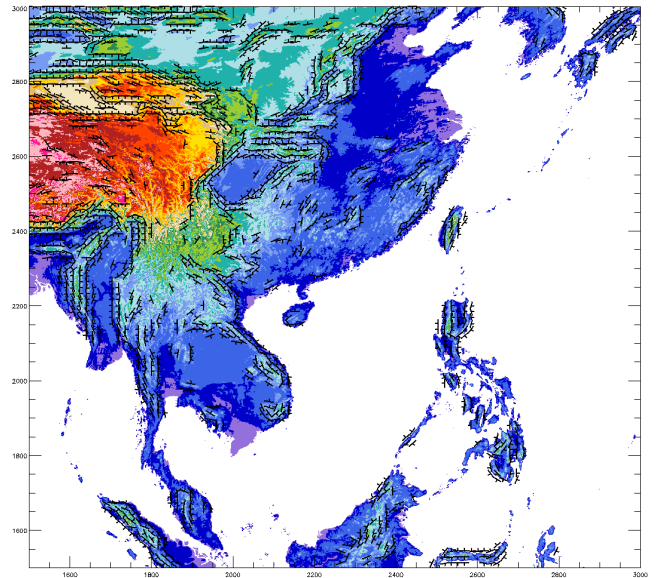


Figure 2. Topography of southeast Asia (color) and diagnosed ridges (black symbols). An outer scale of 50 km is used. Only ridges explaining 50% or more of total 2D variance and possessing maximum vertical displacement of more than 500 m are shown. Long axes of symbols show ridge crests, short appendages indicate direction of greater descent.

the new topography software already available in CAM. Preliminary results from our algorithm are presented in Figure 2.

3 Results

TEXT

3.1 Sample topography smoothing experiments with CAM-SE

HOMME (High-Order Method Modeling Environment; Thomas and Loft, 2005; Dennis et al., 2005)

Figure 5 shows results from AMIP simulations with CAM-SE using different levels of Φ_s smoothing and numerical diffusion of divergent modes. Spurious noise near steep orography is very apparent for certain model configurations and affects important hydrological fields such as precipitation; even surface pressure varies significantly among the model configurations (not shown) which, in turn, affects sea ice extent and other important climate variables.

While it is necessary to smooth topography to remove spurious grid-scale noise, it introduces two problems. Filtering will typically raise ocean points near step orography to non-zero elevation. Perhaps the most striking example is the Andes mountain range that extends one or two grid cells into the Pacific after the filtering operation (see, e.g., Fig-

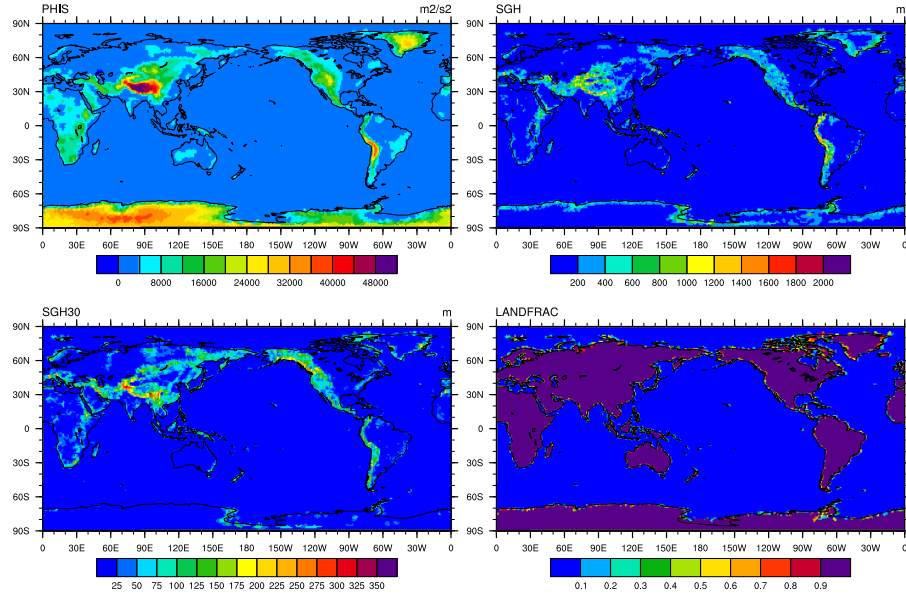


Figure 3. Surface geopotential Φ_s (upper left), SGH (upper right), $SGH30$ (lower left) and $LANDFRAC$ (lower right) for CAM-SE NE30NP4 resolution. The data is plotted on the native grid.

ure ?? right). Ocean and land points are treated separately in weather/climate models so raised sea-points may potentially be problematic. Secondly, the filtering will generally reduce the height of local orographic maxima and given the importance of barrier heights in atmospheric dynamics, this could be a problem for the global angular momentum budget and could fundamentally change the flow.

To capture the barrier effect (blocking) that is sub-grid scale with respect to the smoothed orography, one may use *envelope orography* that adjusts the surface height with sub-grid scale orographic variance (Wallace et al., 1983). Loosely speaking, the peak heights are raised. A similar approach, but implemented as variational filtering, is taken in Rutt et al. (2006); this method also imposes additional constraints such as enforcing zero elevation over ocean masks.

As mentioned above it is not straight forward to determine how to smooth orography. One approach is to try different filtering methods in the full model and evaluate the results in weather forecasts or longer climate simulations (Navarra et al., 1994; Bouteloup, 1995, 1996). While this approach is certainly valuable, clearly the size of the Gibbs oscillations in global spectral models is reduced by smoothing orography, it does not take into account the interaction between the resolved-scale flow (dynamical core) and parameterizations of sub-grid scale processes (e.g., gravity wave drag, turbulent

mountain stress). This interaction can be difficult to predict and commonly the sub-grid scale parameterization have been tuned over a number of years with the ‘default’ smoothed surface elevation. Hence, this methodology runs the risk of deeming one smoothing less accurate than another due to lack of optimum tuning (and/or complexity) of the parameterizations.

Another approach is to use idealized simulation with no parameterizations to determine what scales are adequately resolved and which are poorly resolved. Davies and Brown (2001) kept the physical scale of an idealized two-dimensional and three-dimensional isolated hill fixed and observed how the coarser resolution results differ from the high-resolution simulation. This can then provide guide-lines on how to smooth orography in the full model. Similar idealized (shallow water) experiments were used in Rutt et al. (2006) to optimally smooth orography. While these idealized tests provide a ‘cleaner’ approach to smoothing terrain, they do not consider the coupling with sub-grid scale processes.

TEXT

3.1.1 HEADING

TEXT

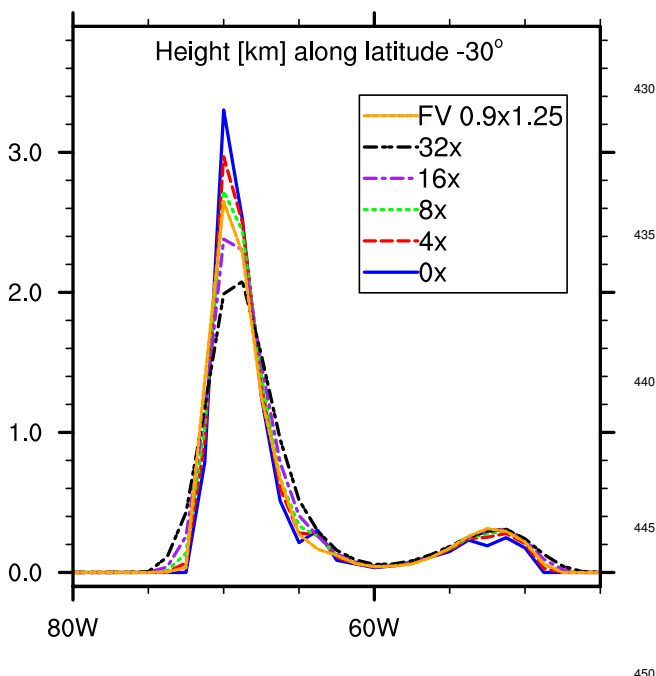


Figure 4. Surface elevation in kilometers for a cross section along latitude 30°S (through Andes mountain range) for different representations of surface elevation. Labels ‘4x’, ‘8x’, ‘16x’ and ‘32x’, refer to different levels of smoothing, more precisely, four, eight, sixteen and thirtytwo applications of a ‘Laplacian’ smoothing operator in CAM-SE, respectively. Label ‘FV 0.9° × 1.25°’ refers to the topography used in CAM-FV. ‘0x’ is the unsmoothed topography on an approximately 1° grid.

4 Conclusions

TEXT

Appendix A:

415

Grid descriptor NetCDF file

A1 asdf

Acknowledgements. NCAR is sponsored by the National Science Foundation (NSF). Thanks to DOE ...

420 References

- Balmino, G.: The Spectra of the topography of the Earth, Venus and Mars, *Geophys. Res. Lett.*, 20, 1063–1066, doi:10.1029/93GL01214, 1993.
- Bouteloup, Y.: Improvement of the Spectral Representation of the Earth Topography with a Variational Method, *Mon. Wea. Rev.*, 123, 1560–1574, 1995.
- Bouteloup, Y.: Optimal Spectral Topography and Its Effect on Model Climate, *J. Climate*, 9, 2443–2463, 1996.
- Davies, L. and Brown, A.: Assessment of which scales of orography can be credibly resolved in a numerical model, *Quart. J. Roy. Meteor. Soc.*, 127, 1225–1237, doi:10.1002/qj.49712757405, 2001.
- Dennis, Fournier, A., Spotz, W. F., St-Cyr, A., Taylor, M. A., Thomas, S. J., and Tufo, H.: High-Resolution Mesh Convergence Properties and Parallel Efficiency of a Spectral Element Atmospheric Dynamical Core, *Int. J. High Perform. Comput. Appl.*, 19, 225–235, doi:10.1177/1094342005056108, 2005.
- Dennis, J. M., Edwards, J., Evans, K. J., Guba, O., Lauritzen, P. H., Mirin, A. A., St-Cyr, A., Taylor, M. A., and Worley, P. H.: CAM-SE: A scalable spectral element dynamical core for the Community Atmosphere Model, *Int. J. High. Perform. C.*, 26, 74–89, doi:10.1177/1094342011428142, <http://hpc.sagepub.com/content/26/1/74.abstract>, 2012.
- Durran, D.: Numerical Methods for Fluid Dynamics: With Applications to Geophysics, vol. 32 of *Texts in Applied Mathematics*, Springer, 2 edn., 516 p., 2010.
- Farr, T. G., Rosen, P. A., Caro, E., Crippen, R., Duren, R., Hensley, S., Kobrick, M., Paller, M., Rodriguez, E., Roth, L., Seal, D., Shaffer, S., Shimada, J., Umland, J., Werner, M., Oskin, M., Burbank, D., and Alsdorf, D.: The Shuttle Radar Topography Mission, *Reviews of Geophysics*, 45, doi:10.1029/2005RG000183, 2007.
- Gesch, D. B. and Larson, K. S.: Techniques for development of global 1-kilometer digital elevation models, in: *Pecora Thirteenth Symposium, Am. Soc. Photogrammetry Remote Sens.*, Sioux Falls, South Dakota, 1998.
- GLOBE Task Team and others: The Global Land One-kilometer Base Elevation (GLOBE) Digital Elevation Model, Version 1.0, <http://www.ngdc.noaa.gov/mgg/topo/globe.html>, 1999.
- Jones, P. W.: First- and Second-Order Conservative Remapping Schemes for Grids in Spherical Coordinates, *Mon. Wea. Rev.*, 127, 2204–2210, 1999.
- Lander, J. and Hoskins, B.: Believable scales and parameterizations in a spectral transform model, *Mon. Wea. Rev.*, 125, 292–303., doi:10.1175/1520-0493, 1997.
- Lauritzen, P. H. and Nair, R. D.: Monotone and conservative Cascade Remapping between Spherical grids (CaRS): Regular latitude-longitude and cubed-sphere grids., *Mon. Wea. Rev.*, 136, 1416–1432, 2008.
- Lauritzen, P. H., Nair, R. D., and Ullrich, P. A.: A conservative semi-Lagrangian multi-tracer transport scheme (CSLAM) on the cubed-sphere grid, *J. Comput. Phys.*, 229, 1401–1424, doi:10.1016/j.jcp.2009.10.036, 2010.
- Lauritzen, P. H., Mirin, A., Truesdale, J., Raeder, K., Anderson, J., Bacmeister, J., and Neale, R. B.: Implementation of new diffusion/filtering operators in the CAM-FV dynamical core, *Int. J. High Perform. Comput. Appl.*, doi:10.1177/1094342011410088, 2011.
- Lin, S.-J.: A ‘Vertically Lagrangian’ Finite-Volume Dynamical Core for Global Models, *Mon. Wea. Rev.*, 132, 2293–2307, 2004.
- Lott, F. and Miller, M. J.: A new subgrid-scale orographic drag parametrization: Its formulation and testing, *Quart. J. Roy. Meteor. Soc.*, 123, 101–127, doi:10.1002/qj.49712353704, 1997.
- Nair, R. D., Thomas, S. J., and Loft, R. D.: A Discontinuous Galerkin Transport Scheme on the Cubed Sphere., *Mon. Wea. Rev.*, 133, 814–828, 2005.

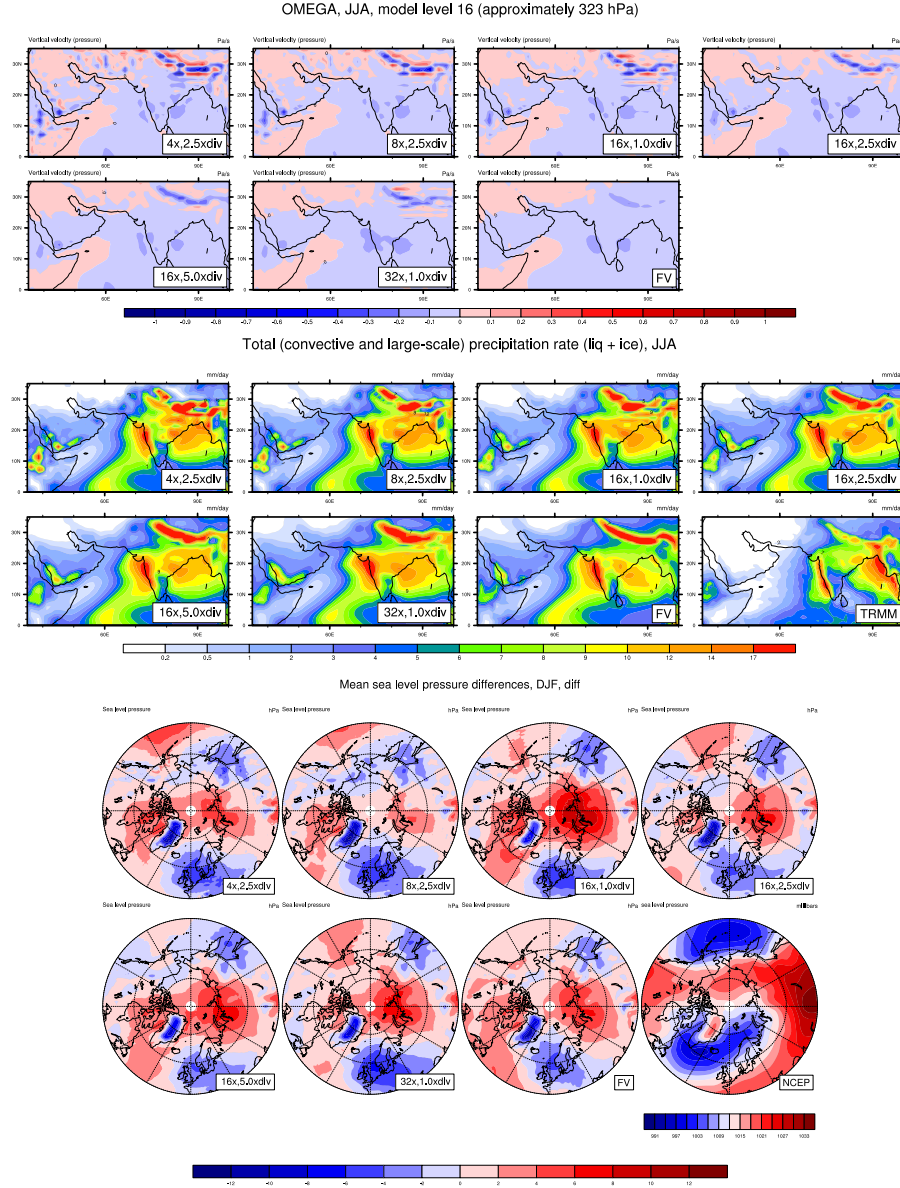


Figure 5. Diagnostics for 30 year AMIP simulations with CAM5.2. Upper, middle and lower group of plots are model level 16 vertical velocity, total precipitation rate and mean sea level pressure differences, respectively. Except for the two right-most plots on the second row of each group of plots, the diagnostics are for CAM-SE with different amounts of smoothing of Φ_s and different levels of divergence damping. The amount of smoothing follows the same notation as Fig. 4 (right) and 1.0xdv, 2.5xdv, 5.0xdv refers to increasing divergence damping by a factor 1.0, 2.5, and 5.0, respectively. The second right-most plot on each group of plots (labeled FV) show results for CAM-FV. Lower right plot in the second and third group of plots show TRMM observations and NCEP reanalysis data, respectively.

Nastrom, G. D. and Gage, K. S.: A Climatology of Atmospheric Wavenumber Spectra of Wind and Temperature Observed by 495 Commercial Aircraft, *J. Atmos. Sci.*, 42, 950–960, 1985.

Navarra, A., Stern, W. F., and Miyakoda, K.: Reduction of the Gibbs Oscillation in Spectral Model Simulations, *J. Climate*, 7, 1169–1183, 1994.

Neale, R. B., Chen, C.-C., Gettelman, A., Lauritzen, P. H., Park, S., Williamson, D. L., Conley, A. J., Garcia, R., Kinnison, D.,

Lamarque, J.-F., Marsh, D., Mills, M., Smith, A. K., Tilmes, S., Vitt, F., Cameron-Smith, P., Collins, W. D., Iacono, M. J., Easter, R. C., Ghan, S. J., Liu, X., Rasch, P. J., and Taylor, M. A.: Description of the NCAR Community Atmosphere Model (CAM 5.0), NCAR Technical Note, National Center of Atmospheric Research, 2010.

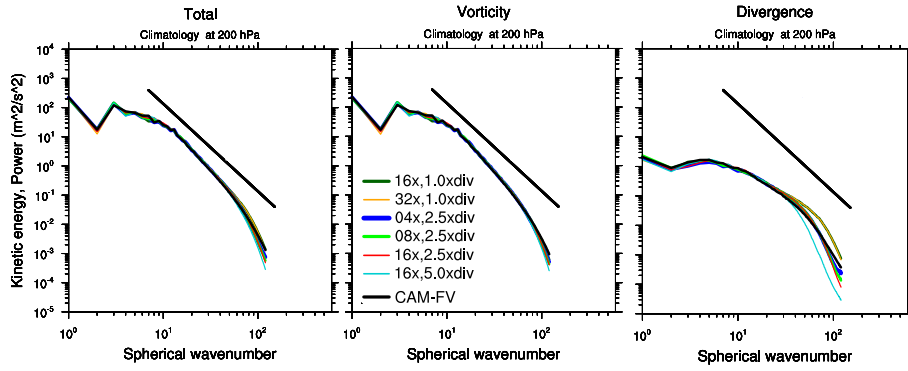


Figure 6. (left) Total kinetic energy spectrum for the velocity field at 200hPa as a function of spherical wavenumber k for CAM-FV and different configurations of CAM-SE. The labeling for the CAM-SE configurations is the same as in Figure 5. The solid-straight black line indicates the k^{-3} reference slope (Nastrom and Gage, 1985). The middle and right plots show the kinetic energy partitioned into divergent and rotational modes, respectively. The spectra have been computed using daily instantaneous wind and surface pressure data for a 2 month period.

- 500 Ronchi, C., Iacono, R., and Paolucci, P. S.: The ‘Cubed Sphere’: A
New Method for the Solution of Partial Differential Equations in
Spherical Geometry, *J. Comput. Phys.*, 124, 93–114, 1996.
Rutt, I., Thuburn, J., and Staniforth, A.: A variational method for
orographic filtering in NWP and climate models, *Quart. J. Roy.
505 Meteor. Soc.*, 132, 1795–1813, doi:10.1256/qj.05.133, 2006.
Thomas, S. J. and Loft, R. D.: The NCAR Spectral Element Cli-
mate Dynamical Core: Semi-Implicit Eulerian Formulation, *J.
Sci. Comput.*, 25, 307–322, 2005.
Ullrich, P. A., Lauritzen, P. H., and Jablonowski, C.: Geometrically
510 Exact Conservative Remapping (GECoRe): Regular latitude-
longitude and cubed-sphere grids., *Mon. Wea. Rev.*, 137, 1721–
1741, 2009.
Wallace, J. M., Tibaldi, S., and Simmons, A. J.: Reduction of sys-
tematic forecast errors in the ECMWF model through the intro-
515 duction of an envelope orography, *Quart. J. Roy. Meteor. Soc.*,
109, 683–717, doi:10.1002/qj.49710946202, 1983.
Webster, S., Brown, A., Cameron, D., and Jones, C.: Improve-
ments to the representation of orography in the Met Office
Unified Model, *Quart. J. Roy. Meteor. Soc.*, 129, 1989–2010,
520 doi:10.1256/qj.02.133, 2003.